Lab on a Chip

Accepted Manuscript

ROYAL SOCIETY OF CHEMISTRY

www.rsc.org/loc

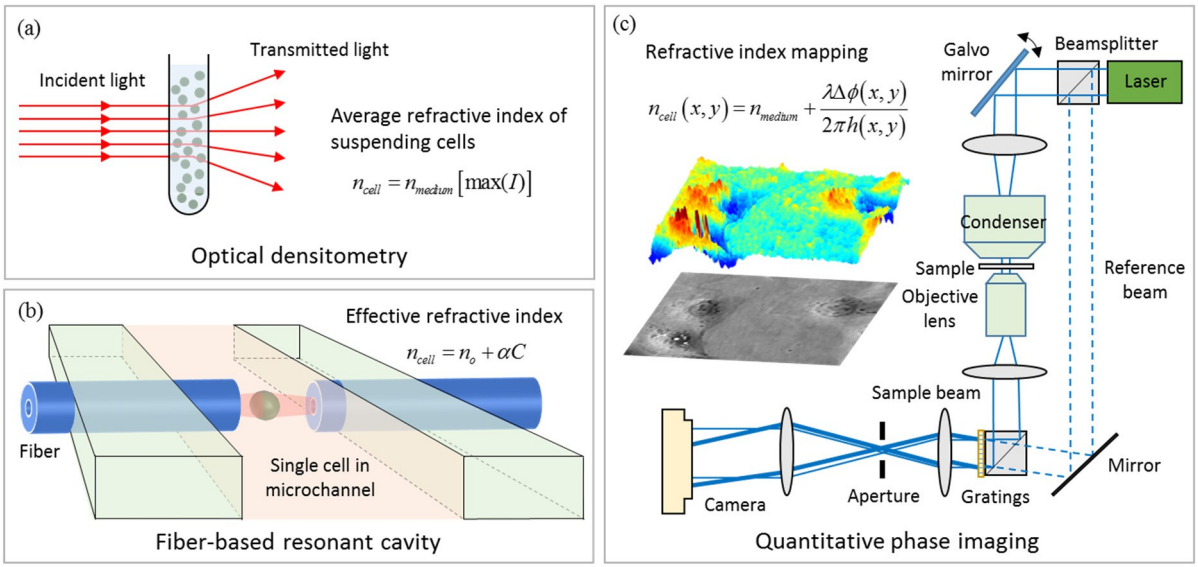

Cell refractive index is an important biophysical parameters, which provides new biological and biomedical insight for disease diagnosis and cell biology.

Cell Refractive Index for Cell Biology and Disease Diagnosis: *Past*, *Present* and *Future*

P. Y. Liu[1,2], L. K. Chin[2†], W. Ser[2†], H. F. Chen[2], C.-M. Hsieh[2], C.-H. Lee[3], K.-B. Sung[4], T. C. Ayi[5], P. H. Yap[6], B. Liedberg[7], K. Wang[8], T. Bourouina[9] and Y. Leprince-Wang[1†]

[1]*Université Paris-Est, UPEM, F-77454 Marne-la-Vallée, France*

[2]*School of Electrical and Electronic Engineering, Nanyang Technological University, Singapore 639798*

[3]*Research Center for Applied Sciences, Academia Sinica, Taipei 11529 Taiwan*

[4]*Department of Electrical Engineering, National Taiwan University, Taipei 106 Taiwan*

[5]*Defence Medical & Environmental Institute, DSO National Laboratories, Singapore 117510*

[6]*Lee Kong Chian School of Medicine, Nanyang Technological University, Singapore 308232*

[7]*Interdisciplinary Graduate School, Nanyang Technological University, Singapore 639798*

[8]*Institute of Biology Chemistry, Academia Sinica, Taipei 115 Taiwan*

[9]*Université Paris-Est, ESYCOM, ESIEE, Paris F-93162 Marne-la-Vallée, France*

([†]lkchin@ntu.edu.sg; ewser@ntu.edu.sg; yamin.leprince@u-pem.fr)

Abstract

Cell refractive index is a key biophysical parameter, which has been extensively studied. It is correlated with other cell biophysical properties including mechanical, electrical and optical properties, and represents not only the intracellular mass and concentration of a cell, but also provides important insight for various biological models. Measurement techniques developed earlier only measure the effective refractive index of a cell or a cell suspension, providing only limited information on cell refractive index and hence hindering its in-depth analysis and correlation. Recently, the emergence of microfluidic, photonic and imaging technologies have enabled the manipulation of a single cell and the 3D refractive index of a single cell down to sub-micron resolution providing powerful tools to study cells based on refractive index. In this review, we provide an overview of cell refractive index models and measurement techniques including microfluidic chip based techniques for the last 50 years, present the applications and significance of cell refractive index in cell biology, hematology, pathology, and discuss future research trends in the field, including 3D imaging methods, integration with microfluidics and its potential applications in new and breakthrough research areas.

Introduction

Cell biophysics uses physical models and theories to study cells, such as the mechanical, electrical and optical properties of cells. Mechanical parameters such as elasticity, adhesive force and speed are studied to analyze how cells respond to forces or migrate by deformation etc. [1]. Electrical parameters such as conductivity, impedance and electromotive force are important for the studies of neural networks such as the propagation of electrical synapses [2]. Similarly, optical parameters such as adsorption, scattering, reflection etc. determine how light propagates in a cell, and these optical parameters are strongly correlated with intracellular mass and concentration [3-4]. One of the most important biophysical properties is the refractive index of a single cell, which has been studied and measured since 1950s. It can be used to determine or correlate with other cell biophysical parameters (such as dry mass, wet mass, protein concentration, elasticity, conductivity etc.), and study certain cell metabolic activities (such as cell division, infection etc.). In fact, cell refractive index is not a stranger for life scientists. In flow cytometry, forward and side scattering intensities are often measured whereby the side scattering intensity is related to the cell refractive index. Optical density is used to correlate with bacteria concentration, which is also dependent on the refractive index of bacteria.

Several models of cell refractive index have been developed in last 50 years based on different measurement techniques, which include (1) the average refractive index of a cell population suspending in a medium; (2) the effective refractive index of a single cell; and (3) the 2D and 3D refractive index of a single cell. The effective refractive index of a single cell is more precise as compared to the average refractive index of a cell

population. However, both models are limited in providing sufficient information for biological applications with only a single refractive index value to represent a cell. More sophisticated and complex optical systems are developed to measure the 2D refractive index profile in a surface layer and, more recently, the 3D refractive index profile of a single cell. Both models provide more in-depth refractive index information down to the sub-micron resolution. With this in-depth refractive index information, biologists and biomedical researchers can use cell refractive index to study a single cell or a group of cells for the applications of cell biology and disease diagnosis, attempting to obtain biological insight in the research of biophysics.

To date, several cell refractometers have demonstrated the synergy of microfluidics with optical imaging systems, which provide several benefits which include (1) manipulating and mixing liquids with high flexibility and stability for cell behavior analysis and long-term cell culture etc., (2) manipulating and trapping cells or even bacteria with high controllability and specificity for single or group cell analysis, and (3) high biocompatibility in term of materials and biochemical processes that enable living cell analysis. Microfluidics with robust cell manipulation techniques and highly controllable culture conditions can facilitate non-contact refractive index measurement and mapping with high precision or even for long term refractive index monitoring.

In this review, we provide an overview of cell refractive index models, starting from the average cell refractive index of suspending cells and the effective refractive index of a single cell to 2D and 3D refractive index of a single cell, and their respective measurement techniques including microfluidic chip based techniques. Next, we review biological insights provided by cell refractive index for various applications such as cell

morphology and growth in cell biology, malaria and anemia disease diagnosis in hematology, and cancer cell and circulating tumor cell detection in pathology. Finally, we discuss the outlook, research trends and applications of cell refractive index, including 3D imaging methods, integration with microfluidics and its potential applications in new and breakthrough research areas.

Cell refractive index models and its measurements

The simplest model of cell refractive index measurement is the average refractive index of cells suspending in a medium (Figure 1a). Suspended cells are assumed to be homogeneous with the same refractive index and the average cell refractive index can be determined either by measuring refractive index change using interference refractometry or optical density using optical densitometry [5]. For interference refractometry, the average refractive index of suspending cells (n_{cell}) can be determined based on the classical mixture equation as $n_{cell} = n_{medium} + \frac{\Delta n}{V_{cell}}$ where n_{medium} is the refractive index of medium, V_{cell} is the volume fraction of cells in the medium and Δn is the refractive index difference measured by interference refractometry. On the other hand, in optical densitometry, the refractive index of the medium is changed incrementally and the optical density is measured. Maximum transmission occurs when the refractive index of the medium and that of the suspending cells are matched. Other methods based on light scattering and transmission were demonstrated [6-7]. The main drawback of this model is its simplicity without any in-depth refractive index information provided. The large variation of cell refractive index within the same cell type cannot be measured and analyzed.

In 1953, R. Barer proposed a more detailed refractive index model based on a single cell [8]. Since a cell is mainly comprised of cytoplasm and proteins occupy the greatest portion of cell solids in the cytoplasm, a single cell is treated as a container filled with a protein solution (Figure 1b). Effective cell refractive index is defined as $n_{cell} = n_o + \alpha C$ where n_o is the refractive index of water or dilute salt solution, α is the specific refraction increment and C is the mass density of protein in gram per deciliter (g/dL) [9-10]. Based on this model, the effective cell refractive index is linearly proportional to the concentration of protein in the cell. Several unconjugated proteins were measured and the specific refraction increment for proteins is $1.845 \times 10^{-3} \pm 0.037 \times 10^{-3}$ [9]. Therefore, the refractive index of a protein solution increases by 1.845×10^{-3} for every one percent increase in the concentration. Most research reports indicate that the refractive index of the protein solution is linear to the concentration of the protein. Barer showed that indeed the variation of refractive index as the protein concentration increases is a linear relationship with an insignificant discrepancy even at high protein concentrations. Although lipids and carbohydrates exist in the cytoplasm but they occur as complexes, which have similar refraction increments as proteins. The influence of pH on the specific refraction increment was investigated and the results showed that the effect of pH is small and negligible [10]. Similarly, the effects of temperature and salt concentration were investigated and their effects on the specific refraction increment are small and within 0.5% to 2% [10].

Several different methods were developed to measure the effective refractive index of a single cell. Immersion refractometry exploits intensity contrast between a cell and its surrounding medium under phase contrast microscopy whereby the cell appears

invisible when its effective refractive index matches with that of the surrounding medium [11]. Similar method integrated in a microfluidic chip was demonstrated to measure the effective refractive index of a single bacterium that is trapped in a microfluidic channel [12]. In addition, several microfluidic chips integrated with various optical techniques were demonstrated to measure the effective refractive index, dry mass and water mass of a single living cell, such as light scattering [13], laser resonant cavity [14], FP resonant cavity [15], grating resonant cavity with optical trap [16], Mach-Zehnder interferometer [17] etc. Resolution up to 10^{-3} refractive index unit (RIU) was demonstrated [16]. Most of these techniques measure the optical path difference caused by the cell in the medium and decouple its effective refractive index and size by differential buffer method [15-17]. The main drawback of these techniques is the assumption of a single living cell as a spherical object filled with a protein solution. In reality, cells exist in different shapes and other organelles exist in the cell especially cell nucleoli that is denser than the cytoplasm. In most cases, minor changes in the concentration and the abundance of various intracellular organelles are not reflected in the effective refractive index. Therefore, the study of effective refractive index does not provide many details to understand sophisticated cell biological processes.

With the recent development in advanced optical imaging systems, the 2D and 3D refractive index of a single cell down to the sub-micron resolution are now feasible and demonstrated (Figure 1c). A cell is no longer treated as a homogeneous entity filled with a protein solution, but an entity with spatial refractive index distribution. Localized surface plasmon excitation by using a near-field probe was developed to obtain the 2D refractive index of cell samples on a focal plane by scanning point-by-point [18, 19]. A

spatial resolution of several tenth nanometers with a resolution of 10^{-5} RIU was demonstrated [19]. However, it is time consuming since scanning point-by-point is required. One new trend for cell refractive index mapping is quantitative phase imaging [20-29]. Phase delay map ($\Delta\phi$) that is diffracted by the cell consists of the structural and optical information of the cell, i.e. $n_{cell}(x,y) = n_{medium} + \frac{\Delta\phi(x,y)\lambda}{2\pi h_{cell}(x,y)}$ where x and y are the spatial coordinates, λ is the wavelength of light and $h_{cell}(x, y)$ is the cell thickness. Since cell refractive index is linearly proportional to the protein concentration, the dry mass density of the cellular matter can be determined as $\sigma(x,y) = \frac{\lambda}{2\pi\alpha}\Delta\phi(x,y)$ where α is the specific refraction increment in ml/g. One of the quantitative phase imaging techniques is based on off-axis configuration whereby reference and sample beams are deviated with a small angle difference, which include digital holographic microscopy [21-22] and Hilbert phase microscopy [23]. The interference image of the cell, resulting from the overlap of the reference and sample beams, is captured and the phase map can be extracted from the interference image through phase unwrapping and background subtraction algorithms. By knowing and making assumption on the shape of the cell, the 2D refractive index profile can be obtained. The demonstrated refractive index resolution was as low as 10^{-4} RIU [22]. Another technique is based on phase-shifting method whereby four phase-shifted interference images ($\pi/2$ per frame) are captured and phase maps are extracted from the interference image through phase unwrapping algorithm [24-25]. Although the off-axis method is fast with a single image, the phase-shifting method maintains diffraction-limited transverse resolution (250 nm). For higher stability down to mrad levels, common-path configuration is demonstrated whereby a diffraction grating is used to

create a reference beam that travels through the same optical path as the sample beam [26]. For the 3D refractive index measurement of a single cell, a series of phase images is captured at various angles and the 3D refractive index profile can be reconstructed by algorithms such as filtered back-projection or optical diffraction tomography [27-28]. Recently, the 3D refractive index measurement of a single cell flowing in a microfluidic channel is demonstrated [29]. In such a system, a series of angular spectra is generated when the cell is passing through a line-focused beam (sample beam of Mach-Zehnder interferometry) via microfluidics. Similarly, the 3D refractive index of the cell can be reconstructed. Achieved specifications of various measurement techniques including tomographic bright-field imaging technique [30] are summarized in Table 1.

Biological insight and applications

With the capability to measure the refractive index of a single cell, the representative position of refractive index in cell biology has been widely studied. Initially, researchers measured the refractive index of different biological samples ranging from tissues and cells to bacteria and viruses. Subsequently, the refractive index of normal cells and abnormal cells were measured and compared to search for the correlation with diseases such as cancers, malaria, anemia, bacterial infection etc. In this section, the applications of refractive index in three different research fields are discussed. They are cell biology, hematology and pathology.

Cell biology

Effective refractive index of various cells has been widely demonstrated and due to many advances in methodology and measurement systems, we are now able to measure the refractive indices of various components of the cell such as cytoplasm and nucleus. For example, live HeLa cells suspended in culture medium were measured by using tomographic phase imaging and the refractive index of the nucleus is between 1.355 - 1.365 RIU, while the refractive index of the cytoplasm is 1.360 - 1.390 RIU and the nucleoli have the highest refractive index at 1.375 - 1.385 RIU [28]. Typical refractive index values of various organelles are shown in Table 2. These results provide new insight in cell biology because, previously, it is widely claimed that the refractive index of nucleus is higher than that of cytoplasm [33]. Similar results are obtained with other cell line such as HEK 293 cells whereby small cytoplasmic particles (possibly lipid droplets, vacuoles or other organelles) with high refractive index are observed.

The refractive index of various bacteria was also widely measured and studied throughout the years. Based on suspension techniques, *E. coli* was measured with an average refractive index of 1.401 and 1.406 RIU by using interference refractometry and optical densitometry, respectively [5]. The measured average refractive index of a suspended *E. coli* is relatively higher than the measured effective refractive index of a single *E. coli*. With immersion refractometry, the effective refractive index of *E. coli* was measured as 1.386 RIU [12]. The basic model of a single *E. coli* was studied whereby the nucleoid, which is clearly visible under phase-contrast microscope, is separated from the cytoplasm. The contrast between the nucleoid and the cytoplasm is resulted from the difference in refractive index and solid concentration. The cytoplasm with RNA (0.5%

wt/vol) and protein (21% wt/vol) has refractive index of 1.390 RIU while the nucleoid mainly with DNA (6.8% wt/vol) and low amount of protein (8.6% wt/vol) has refractive index of 1.371 RIU [34]. In addition, the morphology of bacteria will also affect their refractive index such as bacillus family, which is capable to produce endospore and undergo sporulation. The effective refractive indices of various bacillus bacteria in their vegetative and sporulation forms were measured by using the immersion refractometry. The results showed that bacillus spores (1.517 – 1.539 RIU) have relatively higher effective refractive index than their vegetative forms (1.387 – 1.400 RIU) [35]. This is because the solid content in spore is significantly increased from approximately 30 to 99 g per 100 ml while the water content is reduced from approximately 77.5 to 25.5 g per 100 ml.

Due to the small size of viral particles, the refractive index measurement techniques are limited and mainly based on the suspension measurement. The average refractive index of coliphages and marine phages with capsid size ranging from 25 to 100 nm suspended in phosphate-buffered saline buffer were measured based on light scattering [36]. The results showed that these viruses have a relative average refractive index of 1.025 to 1.177. Due to the limitation of the measurement technique, not much information can be studied to understand viruses based on refractive index.

Since cell refractive index is correlated with the concentration of matters, the first direct application of cell refractive index is cell growth monitoring. In cell cycle (Figure 2a), the cell first enters G1 phase and grows by producing proteins and cytoplasmic organelles, then enters S phase whereby chromosomes are replicated, followed by entering G2 phase to grow more and finally divide in M phase. Since the DNA content in

the nucleus is doubled in the G2/M phases as compared to the G1/S phases, the nuclear refractive index of HeLa cells (trypsinized and resuspended in Cytolyt, solidified by HistoGel and fixed in 10% formalin) were measured and shown to be increased from 1.5495 to 1.5515 RIU (Figure 2b) [37]. The growth of human osteosarcoma (U2OS) cells was also studied and they were transfected with YFP-proliferating cell nuclear antigen (PCNA) to monitor its progression through the S phase [38]. From the results, U2OS cells exhibited clear exponential growth in the G2 phase and typically doubled their mass by the end of the G2 phase (Figure 2c). After mitosis, daughter cells are typically half of their parents' doubled mass. Similar observation was recorded for the growth of *E. coli*. During the growth, *E. coli* underwent binary fission whereby DNA was replicated, its size was increased and new daughter cells were formed with the complete development of the new cell wall. The growth rate of *E. coli* was shown to be linearly proportional to cell mass, which indicated the exponential growth behavior of *E. coli*. The nuclear division during binary fission was also observed by the immersion refractometry [39]. The cycle started as sister nuclei were separated, forming a septum. The nucleus appeared like a 3-lobed structure. The individual lobes divided as they remained connected together. Then, the nuclear lobes moved apart, and the sister cells were completely separated at the opposite ends of the cell. This cell cycle continued for a new division for thirty minutes. On the other hand, cell-surface interaction can also be quantified by using a photonic crystal enhanced microscopy with sufficient spatial resolution to monitor cell membrane and intra-cell attachment distribution, and temporal resolution to investigate different biological processes such as chemotaxis, apoptosis, differentiation and division [40].

Hematology

There are several types of cells in blood stream, which include red blood cells, white blood cells and platelets. Red blood cells are oval biconcave disks with relatively simpler cell structure. They are lack of a cell nucleus and most organelles but rich in hemoglobin. Based on tomographic bright field imaging, red blood cells have a mean refractive index of 1.402, a dry mass of 27.2 pg, a diameter of 7.0 μm, a volume of 100.7 fL and a density of 27.1 pg/fL [30].

Similarly, the platelets that help sustain hemostatic and arterial thrombosis especially fibrillation are subcellular fragment of blood without a cell nucleus. The two types of platelets that help separate between healthy and unhealthy individuals with diseases are in the form of activated and inactivated platelets. In the activated state, the platelets have spherical needle-like structure, while the inactivated state is a discoid shape with a diameter of 2 – 4 μm and a thickness of 0.5 – 2 μm [41]. During activation whereby oxygen enters into blood plasma, a temporary protrusion results in spherical platelet cell. Due to this difference, platelets are a useful means to determine certain diseases such as cerebrovascular disease, ischemic heart disease and renovascular disease [42-44]. The refractive index of the platelet cell was measured as 1.390 RIU in the range of 1.360 - 1.409 RIU [41, 45].

On the other hand, white blood cells are the body's main line of defense. There are five types of white blood cells in the blood stream, i.e. lymphocytes, monocytes, eosinophils, basophils, and neutrophils. Their sizes are in the range of 6 – 10 μm. Lymphocytes have a relatively simpler structure with a nucleus and a small amount of

cytoplasm, monocytes has a kidney-shaped nucleus, and others have a multilobed nucleus and granules in the cytoplasm as shown in Figure 3a [46]. Based on light scattering and multiple-layer spherical models, lymphocytes and monocytes were measured to have a nuclear refractive index of 1.43 ± 0.05 RIU and 1.43 ± 0.04 RIU, respectively; and a cytoplasmic refractive index of 1.356 ± 0.009 RIU and 1.348 ± 0.004 RIU, respectively [47]. Based on immersion refractometry, lymphocytes were measured with a cytoplasmic refractive index of 1.3572 RIU [48], which is lower than the one measured by the light scattering because of the effective refractive index model. Researchers showed that lymphocytes from infected or vaccine injected animals have a higher refractive index equivalent to 1% to 2% of the protein concentration due to the production of antibodies [49-50].

As human red blood cells are lack of a nucleus and cellular organelles, by obtaining the refractive index of the cytoplasm of the red blood cells, the concentration of hemoglobin can be determined, i.e. $n_{rbc} - n_o = \beta C_{hemoglobin}$ where n_o = 1.335 is the refractive index of cell fluid without hemoglobin and β = 0.0019 dL/g [51]. The hemoglobin concentration for hypochromic anemia patients is relatively lower (37.9 vs 27.4 g/dL). On the other hand, for sickle cell anemia whereby the red blood cell is distorted into a crescent shape and has a stiffer cell membrane, the stiffness of the red blood cell can be determined by dynamically measuring the fluctuation of the cell membrane using quantitative phase imaging [52]. Another major disease of red blood cell is malaria with 250 million people infected yearly. Hence, it is crucial to detect malaria more effectively, allowing early treatment and reducing fatality. Malaria is caused by a protozoan parasite, transmitted by mosquitoes that invade liver cells and red blood cells.

Four species of *plasmodium* can infect humans and cause malaria, i.e. *Plasmodium falciparum (P. falciparum), P. vivax, P. malariae and P. oval*. However, not all the species are fatal in which only *P. falciparum* caused malaria leads to lethal infection and results in the most deaths, while *P. vivax* leads to severe disability after infection. Malaria infection cycle starts when mosquito feed on people. As the mosquitoes feed on human blood, malaria parasites called sporozoites are injected into human tissues. The sporozoites travel to the blood stream and invade the liver cells, which are called hepatocytes. As the hepatocytes burst, the parasites are released into the bloodstream as merozoites to attack the red blood cells and start an intraerythrocytic cycle as shown in Figure 3b [53]. The intraerythrocytic cycle causes structural, biochemical and mechanical changes to the red blood cells. The cycle starts from the ring stage at which the merozoites invade the red blood cells and become uni-necleated trophozoites. At schizont stage, trophozoites develop into multi-nuclei cells called schizonts. The growth of the schizonts is based on the digestion of hemoglobin with the production of hemozoin [54]. These schizonts undergo differentiation to form multiple merozoite cells in the red blood cell, and the discocyte shape of the red blood cell is lost during progression to the scizont stage. The tomographic phase microscopy is used to determine the refractive index change in the red blood cells after *P. falciparum* infection through all the different stages; from healthy red blood cells to ring stage, trophozoite and schizont stage [55]. Healthy red blood cells have a homogeneous distribution in refractive index, while infected red blood cells show non-homogeneous refractive index throughout the cytoplasm of the cell. The lack of homogeneity in the infected blood cells may be due to several different factors; such as hemoglobin is metabolized and transformed into hemozoin crystal in the

P. falciparum membrane. The vacuole of parasite occupies part of the cytoplasm of the red blood cells and several types of parasite proteins are transferred from the parasite into the cytoplasm of the infected red blood cells. Parasites cause changes to both the internal and membrane structure of the red blood cells. There is a significant refractive index difference between the healthy and the infected red blood cells. The healthy red blood cells have refractive index of 1.399 ± 0.006 RIU, whereas the infected red blood cells have a refractive index of 1.395 ± 0.005 RIU in the ring stage, 1.383 ± 0.005 RIU in the trophozoite stage, and finally 1.373 ± 0.006 RIU in the schizont stage [55]. This indicates a significant decreasing trend in the refractive index of the red blood cells during the infection process. The decrement of refractive index of the infected red blood cells is correlated with the decrease in the hemoglobin concentration. As the infection proceeds, the cyptoplasm volume reduces as compared to the healthy red blood cells. As a result, the red blood cell's refractive index and morphology can be used as important parameters for disease diagnosis such as malaria and anemia. In addition, the refractive index of various cells in blood sample can be further studied and developed as one of the indicators in hematology laboratory diagnosis.

Pathology

Certain abnormalities identified in cancer cells are increased nuclear size, irregular shape and uneven chromatin texture [56]. Based on these characteristics along with the advancements in nanoscale detection techniques, prognosis and early detection is becoming a real possibility. Various researches have characterized the refractive index of normal and cancer cells, aiming to better understand the abnormal cell cycles and

increased proliferation of the cancer cells. Most normal cells have a refractive index of 1.353 RIU and cancer cells have a higher refractive index ranging from 1.370 to 1.400 RIU [14, 57]. As many human cancer cells show atypical cell cycles and increase in cell proliferation, the increase in the refractive index may be related to the increase in cell production during various stages of cell cycle in cancer patients. Specimens of breast biopsies were studied by measuring the cell refractive index using the spatial-domain low-coherence quantitative phase microscopy [58]. Three groups of cells were measured, i.e. normal cells, uninvolved cells (cancer cells that are diagnosed as normal cells) and malignant cells. The results showed that the nuclear refractive index is increased from 1.542, 1.544 to 1.545 RIU, suggesting the nuclear refractive index may be an important parameter for early-stage cancer diagnosis. Clinical studies show that circulating tumor cells (CTCs) are present in the blood stream when cancer metastasis occurs. The concentration of CTCs in the blood stream is critical and correlated with the overall survivor rate of cancers such as breast, prostate and colorectal. However, the concentration of CTCs (10 per ml) are relatively very low as compared to white blood cells (10^6 per ml) and red blood cells (10^9 per ml), which significantly increase the difficulties in detecting CTCs. The biophysical properties of CTCs and leukocytes in an ovarian cancer patient were measured and compared by using the quantitative phase imaging [59]. The results showed that CTCs have a higher mass (33.6 vs 18.7 pg), a greater volume (518.2 vs 230.0 fL) and a lower dry mass density (0.065 vs 0.085 pg/fL) as compared to leukocytes (Figure 4a). These results provide insight into the development of a label-free biophysical CTC detection system, and aiding to understand the genetic and proteomic composition of CTCs for targeted therapies.

Prevention of parasite infection through the detection of bacteria and virus in water and food has been an ongoing process with vast improvements over the years due to new technologies that reduce the amount of detection time and costs. The current standard method used for bacteria detection in drinking water is the USEPA Method 1604 [60]. Several technological limitations exist in this method that impedes its effectiveness in preventing a bacteria outbreak, such as laboratory-based and long processing time. Hence, much effort is made to reduce the amount of detection time and find a more cost effective on-site method. Several potential methods have come up and one of them is using the refractive index and morphology of different bacteria to correctly identify the source of an infection [61]. An on-chip optofluidic refractometry [12] that can detect the refractive index and morphology of a single bacterium in real-time was demonstrated for the characterization of three different bacteria species, i.e. *E. coli*, *shigella flexneri* and *vibrio cholera* (Figure 4b). The results showed that the three bacteria have distinctive refractive index values, demonstrating the potential applications of using refractive index for bacteria identification by building up a morphology and refractive index database.

The quantitative phase microscopy was also used to monitor the refractive index change of infected host cells such as *Salmonella*-infected bone marrow derived macrophage [62]. In one study, the dynamic cell morphological changes of rat basophilic leukemia RBL-2H3 cells infected with *vibrio vulnificus* strains were investigated [63]. The results showed that infected RBL-2H3 cells increased gradually after infection due to the influx of water through micropores formed on the membrane affected by the infection. Typically, around 76 mins after infection, cell volume showed an

unrecoverable sharp decline, which is presumably due to the irreversible cell death process.

Outlook for cell refractive index

Cell refractive index is a fundamental biophysical parameter that correlated to the intracellular contents, cell size and mass etc. It is critical to consider the following criteria when cell refractive index is used for cell analysis and disease diagnosis:

(1) *Statistical sample size* - cell refractive index, size and mass etc. vary in range even for the same cell species. In such a case, it may not be conclusive to determine cell types or states with a limited number of cells. To extract meaningful and correlated information from the cell refractive index, it is essential to have a sufficiently large number of cells.

(2) *Non-specificity* – Unlike other label-free techniques such as coherent anti-Stoke Raman scattering, cell refractive index is non-specific to chemical or protein molecules. However, it has a huge potential in complement to existing biochemical techniques such as fluorescence biomarkers to provide a more complete information on the target specimens. Most techniques for the measurement of cell refractive index are compatible and can be easily integrated with fluorescence detection. With specificity provided by fluorescence biomarkers, more in-depth analysis of cell refractive index on cell biology and disease diagnosis can be performed.

(3) *Dependent on measurement conditions* – The measurement of cell refractive index is greatly depending on the chemical pre-treatments and extracellular conditions such as live or fixed samples, chemical treatments, temperature, osmotic pressure, culture medium etc. For example, the nuclear refractive index of live and fixed HeLa cells was

measured with values of 1.355-1.365 [28] and 1.550-1.552 [37], respectively. Therefore, for any investigation to correlate cell refractive index with cell state or disease diagnosis, experimental conditions have to be controlled and maintained throughout the experiments.

(4) *Lateral resolution* – Previously, only average refractive index of suspending cells or effective refractive index of single cell can be measured, which limit the applications of cell refractive index due to the lack of details and resolution. With the advanced development of optical imaging techniques, cell refractive index mapping offers substantial resolution and detailed information for the studies of cell biology, hematology and pathology. Not only diffraction limited lateral resolution is preserved, rapid temporal resolution and 3D life cell imaging can also be realized. However, the diffraction limit of lateral resolution may hinder the applications of cell refractometry for nano-sized viral particle in virological studies or single molecule or sub-cellular organelle analysis. Similar to super-resolution fluorescence imaging techniques, which can image labelled samples beyond diffraction limit to several tenth of nanometer, phase nanoscopy is the future trends of cell refractometry for technological and scientific breakthrough. Indeed, a time-lapse phase nanoscopy with a lateral phase resolution of 90 nm is developed [64], which is used a nanoscale aperture with a diameter of 75 nm to improve the light quality, leading to the improved lateral resolution.

On the other hand, robust and high throughput manipulation methods for cells and liquids in microfluidic platforms have gained more attention in the research community of cell refractometry. Microfluidics is employed not only to deliver a single cell into resonant cavities for effective cell refractive index measurements, but also to control the flow of cells, passing through the sample beam of quantitative phase imaging, and

generate a time sequence of interference images for 3D refractive index mapping [29]. The integration of advanced optical imaging techniques in the microfluidic platform can also facilitate the dynamic studies of cultured cells. Applications such as localized chemical or optical stimulation of patterned neuron networks in a microfluidic chip [65-66], the mechanical motions of cancer cells through structural barriers [67], the effect of cells under constant and pulsatile shear stresses and chemical stimulants [68-69] are among the important biomedical research areas of microfluidics. By combining with advanced optical imaging techniques to measure and monitor the refractive index distribution of cells, new biological insight will be obtained since localized changes down to 100-nm can be easily measured. One specific interesting area is the application of cell refractive index in a flow cytometry. Current flow cytometry only uses scattering signals as a parameter for gating without providing much information on the sample. With the advanced development in cell refractive index measurement technique, in future, cell refractive index and size can replace scattering signals to provide direct information on tested sample in complement to fluorescence signals. Another application will be long-period cell monitoring in the microfluidic platform for disease diagnosis. For example, the changes of host cell morphology and intracellular organelles can be monitored and studied by using 2D refractive index mapping in high spatiotemporal resolutions during virus infection to investigate the infection cycle and aim to develop a rapid virus infectivity technique.

Conclusions

Cell refractive index is one of the key biophysical parameters extensively studied starting from the average refractive index of suspending cells and the effective refractive index of a single cell to the recent 2D and 3D refractive index of a single cell. With the development of advanced optical imaging techniques to measure cell refractive index with an ultra-high spatial resolution (100-nm), various new biological insights are provided by studying cell refractive index, such as cell morphology and growth in cell biology, malaria and anemia disease diagnosis in hematology, and cancer cell and circulating tumor cell detection in pathology. The synergy between microfluidics and cell refractometry has pushed such cutting-edge research to high-throughput and high-controllability cell dynamics monitoring using optical imaging techniques with high temporal, spatial and axial resolutions. The continuous efforts to improve its spatial and axial resolutions and extending its applications to water and environmental monitoring, food safety monitoring, other biomedical and biological areas such as virology and single molecule analysis will be the main future trends.

Acknowledgements

This work was supported by the Singapore National Research Foundation under its Environmental & Water Technologies Strategic Research Programme (1102-IRIS-05-01/02/04/05), which is administered by the Environment & Water Industry Programme Office (EWI) of the PUB.

References

[1] G. Bao and S. Suresh, *Nature Materials*, 2, 2003, 715-725.

[2] E. S. Boyden, F. Zhang, E. Bamberg, G. Nagel and K. Deisseroth, *Nature Neuroscience*, 8, 2005, 1263-1268.

[3] F. D. Bryant, B. A. Seiber and P. Latimer, *Archives of Biochemistry and Biophysics*, 135,1969, 79-108.

[4] A. H. Hielscher, J. R. mourant and I. J. Bigio, *Applied optics*, 36, 1997, 125-135.

[5] J. B. Bateman, J. Wagman and E. L. Carstensen, *Kolloid-Zeitschrift und Zeitschrift für Polymere*, 208, 1966, 44-58.

[6] A. E. Balaev, K. N. Dvoretski and V. A. Doubrovski, *Proceedings of SPIE*, 4707, 2002, 253-260.

[7] P. S. Tuminello, E. T. Arakawa, B. N. Khare, J. M. Wrobel, M. R. Querry, and M. E. Milham, *Applied Optics*, 36, 1997, 2818-2824.

[8] R. Barer, *Journal of the Optical Society of America*, 47, 1957, 545-556.

[9] R. Barer, K. F. A. Ross and S. Tkaczyk, *Nature*, 171, 1953, 720-724.

[10] R. Barer and S. Joseph, *Quarterly Journal of Microscopical Science*, 95, 1954, 399-423.

[11] S. Joseph, *Journal of Microscopy*, 131, 1983, 163-172.

[12] P. Y. Liu, L. K. Chin, W. Ser, T. C. Ayi, P. H. Yap, T. Bourouina and Y. Leprince-Wang, *Lab on a Chip*, 14, 2014, 4237-4243.

[13] R. A. Flynn, B. Shao, M. Chachisvilis, M Qzkan and S. C. Esener, *Biomedical Microdevices*, **7**, 2005, 93-97.

[14] X. J. Liang, A. Q. Liu, C. S. Lim, T. C. Ayi and P. H. Yap, *Sensors and Actuators A*, 133, 2007, 349-354.

[15] W. Z. Song, X. M. Zhang, A. Q. Liu, C. S. Lim, P. H. Yap and H. M. M. Hosseini, *Applied Physics Letters*, 89, 2006, 203901.

[16] L. K. Chin, A. Q. Liu, X. M. Zhang, C. S. Lim, J. H. Ng, J. Z. Hao and S. Takahashi, *Applied Physics Letters*, 91, 2007, 243901.

[17] W. Z. Song, A. Q. Liu, S. Swaminathan, C. S. Lim, P. H. Yap and T. C. Ayi, *Applied Physics Letters*, 91, 2007, 223902.

[18] K. J. Moh, X. C. Yuan, J. Bu, S. W. Zhu and B. Z. Gao, *Optics Express*, 16, 2008, 20734-20740.

[19] J. Lee, C. Lee, E. Lin and P. Wei, *Applied Physics Letters*, 93, 2008, 173110.

[20] C. L. Curl, C. J. Bellair, T. Harris, B. E. Allman, P. J. Harris, A. G. Stewart, A. Roberts, K. A. Nugent, L. M. Delbridge, *Cytometry Part A*, 65, 2005, 88-92.

[21] F. Charrière, A. marian, F. Montfort, J. Kuehn, T. Colomb, E. Cuche, P. Marquet and C. Depeursinge, *Optics Letters*, 31, 2006, 178-180.

[22] B. Rappaz, P. Marquet, E. Cuche, Y. Emery, C. Depeursinge and P. J. Magistretti, *Optics Express*, 13, 2005, 9361-9373.

[23] N. Lue, W. Choi, G. Popescu, Z. Yaqoob, K. Badizadegan, R. R. Dasari and M. S. Feld, *Journal of Physical Chemistry A*, 113, 2009, 13327-13330.

[24] J.-W. Su, W.-C. Hsu, C.-Y. Chou, C.-H. Chang and K.-B. Sung, *Journal of Biophotonics*, 6, 2013, 416-424.

[25] Y.-C. Chua, W.-Y. Chang, K.-H. Chen, J.-H. Chen, B.-C. Tsai and K. Y. Hsu, *Optik*, 125, 2014, 3307-3310.

[26] W.-C. Hsu, J.-W. Su, T.-Y. Tseng and K.-B. Sung, *Optics Letters*, 39, 2014, 2210-2213.

[27] N. M. Dragomir, X. M. Goh and A. Roberts, *Microscopic Research and Technology,* 1, 2008, 5-10.

[28] W. Choi, C. Fang-Yen, K. Badizadegan, S. Oh, N. Lue, R. R. Dasari and M. S. Feld, *Nature Methods*, 4, 2007, 717-719.

[29] Y. Sung, N. Lue, B. Hamza, J. Martel, D. Irimia, R. R. Dasari, W. Choi, Z. Yaqoob and P. So, *Physics Reviews Applied*, 1, 2014, 014002.

[30] K. G. Phillips, S. L. Jacques and O. J. T. McCarty, *Physics Reviews Letters*, 109, 2012, 118105.

[31] K. Haseda, K. KAnematcu, K. Noguchi, H. Saito, N. Umeda and Y. Ohta, Biomedical Optics Express, 6, 2015, 859-869.

[32] J. D. Wilson, W. J. Cottrell and T. H. Foster, Journal of Biomedical Optics, 12, 2007, 014010.

[33] A. Brunsting and P. F. Mullaney, *Biophysical Journal*, 14, 1974, 439-453.

[34] J. A. Valkenburg and C. L. Woldringh, *Journal of Bacteriology*, 160, 1984, 1151-1157.

[35] K. F. A. Ross and E. Billing, *Journal of General Microbiology*, 16, 1957, 418-425.

[36] W. M. Balch, J. Vaughn, J. Novotny, D. T. Drapeau, R. Vaillancourt, J. Lapierre and A. Ashe, *Limnology Oceanography*, 45, 2000, 492-298.

[37] R. K. Bista, S. Uttam, P. Wang, K. Staton, S. Choi, C. J. Bakkenist, D. J. Hartman, R. E. Brand and Y. Liu, *Journal of Biomedical Optics*, 16, 2011, 070503.

[38] M. Mira,. Z. Wang, Z. Shen, M. Bednarz, R. Bashira, I. Golding, S. G. Prasant and G. Popescu, *Proceedings of the National Academy of Sciences*, 108, 2011, 13124-13129.

[39] D. J. Mason and D. M. Powelson, *Journal of Bacteriology*, 71, 1956, 474-479.

[40] W. Chen, K. D. Long, M. Lu, V. Chaudhery, H. Yu, J. S. Choi, J. Polans, Y. Zhuo, B. A. C. Harley and B. T. Cunningham, *Analyst*, 138, 2013, 5886-5894.

[41] I. V. Kolesnikova, S. V. Potapov, M. A. Yurkin, A. G. Hoekstra, V. P. Maltsev and K. A. Semyanov, *Journal of Quantitative Spectroscopy and Radiative Transfer*, 102, 2006, 37-45.

[42] D. D. McManus and J. E. Freedman, Nature Review Cardiology, *Nature Reviews Cardiology*, 2015, Advance online publication.

[43] L. Vizioli, S. Muscari and A. Muscari, *International Journal of Clinical Practice*, 63, 2009, 1509-1515.

[44] J. T. Daugirdas and A. A. Bernardo, *Kidney International*, 82, 2012, 147-157.

[45] A. E. Moskalensky, M. A. Yurkin, A. I. Konokhova, D. I. Strokotov, V. M. Nekrasov, A. V. Chernyshev, G. A. Tsvetovskaya, E. D. Chikova, and V. P. Maltsev, *Journal of Biomedical Optics*, 18, 2013, 017001.

[46] J. Yoon, K. Kim, H. Park, C. Choi, S. Jang and Y. Park, *Biomedical Optics Express*, 6, 2015, 3865-3875.

[47] V. P. Maltsev, A. G. Hoekstra and M. A. Yurkin, Optics of White Blood Cells: Optical Models, Simulations, and Experiments, in Advanced Optical Flow Cytometry: Methods and Disease Diagnoses (ed V. V. Tuchin), Wiley-VCH Verlag GmbH & Co. KGaA, Weinheim, Germany, 2011.

[48] K. W. Keohane and W. K. Metcalf, *Quarterly Journal of Experimental Physiology*, 44, 1959, 343-350.

[49] J. G. Wilde and W. K. Metcalf, *Annals of Clinical and Laboratory Science*, 5, 1975, 23-26.

[50] K. W. Keohane and W. K. Metcalf, *Nature*, 183, 1959, 4655.

[51] N. Ghosh, P. Buddhiwant, A. Uppal, S. K. Majumder, H. S. Patel and P. K. Gupta, *Applied Physics Letters*, 88, 2006, 084101.

[52] N. T. Shaked, L. L. Satterwhite, M. J. Telen, G. A. Truskey and A. Wax, *Journal of Biomedical Optics*, 16, 2011, 030506.

[53] K. Haldar, S. Kamoun, N. L. Hiller, S. Bhattacharje and C. van Ooij, *Nature Reviews Microbiology*, 4, 2006, 922-931.

[54] I. Weissbuch and L. Leiserowitz, *Chemical Reviews*, 108, 2008, 4899-4914.

[55] Y. Park, M. Diez-Silva, G. Popescu, G. Lykotrafitis, W. Choi, M. S. Feld and S. Suresh, *Proceedings of the National Academy of Sciences*, 105, 2008, 13730-13735.

[56] S. Suresh, *Acta Materialia*, 55, 2007, 3989-4014.

[57] W. J. Choi, D. I. Jeon, S.-G. Ahn, J.-H. Yoon, S. Kim and B. H. Lee, *Optics Express*, 18, 2010, 23285-23295.

[58] P. Wang, R. Bista, R. Bhargava, R. E. Brand and Y. Liu, *Optics Letters*, 35, 2010, 2840-2842.

[59] K. G. Phillips, C. RuizVelasco, J. Li, A. Kolatkar, M. Luttgen, K. Bethel, B. Duggan, P. Kuhn and O. J.T. McCarty, *Frontiers in Oncology*, 2, 2012, 1-8.

[60] J. Olstadt, J. J. Schauer, J. Standridge and S. Kluender, *Journal of Water and Health*, 5, 2007, 267-282.

[61] Y. Jo, J. Jung, J. W. Lee, D. Shin, H. Park, K. T. Nam, J.-H. Park and Y. Park, *Scientific Reports*, 4, 2014, 5090.

[62] A. E. Ekpenyong, S. M. Man, S. Achouri, C. E. Bryant, J. Guck and K. J. Chalut, *Journal of Biophotonics*, 6, 2013, 393-397.

[63] S. Lee, Y. R. Kim, J. Y. Lee, J. H. Rhee, C. S. Park and D. Y. Kim, *Journal of Biomedical Optics*, 16, 2011, 036004.

[64] Y. Cotte, F. Toy, P. JOurdain, N. Pavillon, D. Boss, P. Magistretti, P. Marquet and C. Depeursinge, *Nature Photonics*, 7, 2013, 113-117.

[65] J. El-Ali, P. K. Sorger and K. F. Jensen, *Nature*, 442, 2006, 403-411.

[66] L. J. Millet, M. E. Stewart, R. G. Nuzzo and M. U. Gillette, *Lab on a Chip*, 10, 2007, 1525-1535.

[67] Y. Fu, L. K. Chin, T. Bourouina, A. Q. Liu and A. M. J. VanDongen, *Lab on a Chip*, 12, 2012, 3774–3778.

[68] L. K. Chin, J. Q. Yu, Y. Fu, T. Yu, A. Q. Liu and K. Q. Luo, *Lab on a Chip*, 11, 2011, 1856-1863.

[69] J. Q. Yu, X. F. Liu, L. K. Chin, A. Q. Liu and K. Q. Luo, *Lab on a Chip*, 13, 2013, 2693-2700.

List of Captions

Figure 1: Cell refractive index models: (a) average refractive index of cells suspended in a medium measured by optical densitometry, (b) effective refractive index of a single cell measured by resonant cavity, and (c) refractive index mapping measured by quantitative phase microscopy.

Figure 2: Cell cycle vs refractive index: (a) typical cell cycle whereby cell grows in G_1 phase, DNA replicates in S phase and cell continue to grow in G_2 phase, following by cell division in M phase. (b) Flow cytometry and corresponding nuclear refractive index histogram of HeLa cells arrested at the G1/S and G2/M phases, and statistical analysis of the refractive index from the cell nuclei. (Reprinted with permission from ref. 37. Copyright 2011 SPIE.) (c) U2OS growth over 2 days whereby A shows the dry mass density maps of a single U2OS cell over a cell cycle, B shows the GFP fluorescence images indicating PCNA activity, and C shows the dry mass vs. time for a cell family from 1 cell being divided to 2 and then to 4. (Reprinted with permission from ref. 38. Copyright 2011 PNAS.)

Figure 3: Applications of cell refractive index in hematology. (a) Rendered iso-surfaces of the refractive index map of lymphocyte and macrophage from the cross-sectional images of 3D refractive index tomograms on various axial planes. (Reprinted with permission from ref. 46. Copyright 2015 OSA Publishing.) (b) Schematic illustration of the intraerythrocytic cycle of malaria infection (Reprinted with permission from ref. 53. Copyright 2006 Nature.) and its 3D phase mapping at various stages (A: healthy cell, B:

Ring stage, C: trophozoite stage, and D: Schizont stage) with black arrows indicating the merozoite and gray arrow indicating the hemozoin. (Reprinted with permission from ref. 55. Copyright 2008 PNAS.)

Figure 4: (a) Quantitative phase microscopy of circulating tumor cells (CK+CD45-DAPI+HD-CTC5 and the statistical analysis of density, mass, volume and area comparison between white blood cells and CTC. (Reprinted with permission from ref. 59. Copyright 2012 Frontiers.) (b) Optofluidic immersion refractometer to measure the effective refractive index of single bacterium by varying the external medium to match the one of the bacterium. (Reprinted with permission from ref. 12. Copyright 2014 RSC Publishing.)

Table 1: Cell refractive index models and various measurement techniques.

Table 2: Typical refractive index value for various organelles in a cell.

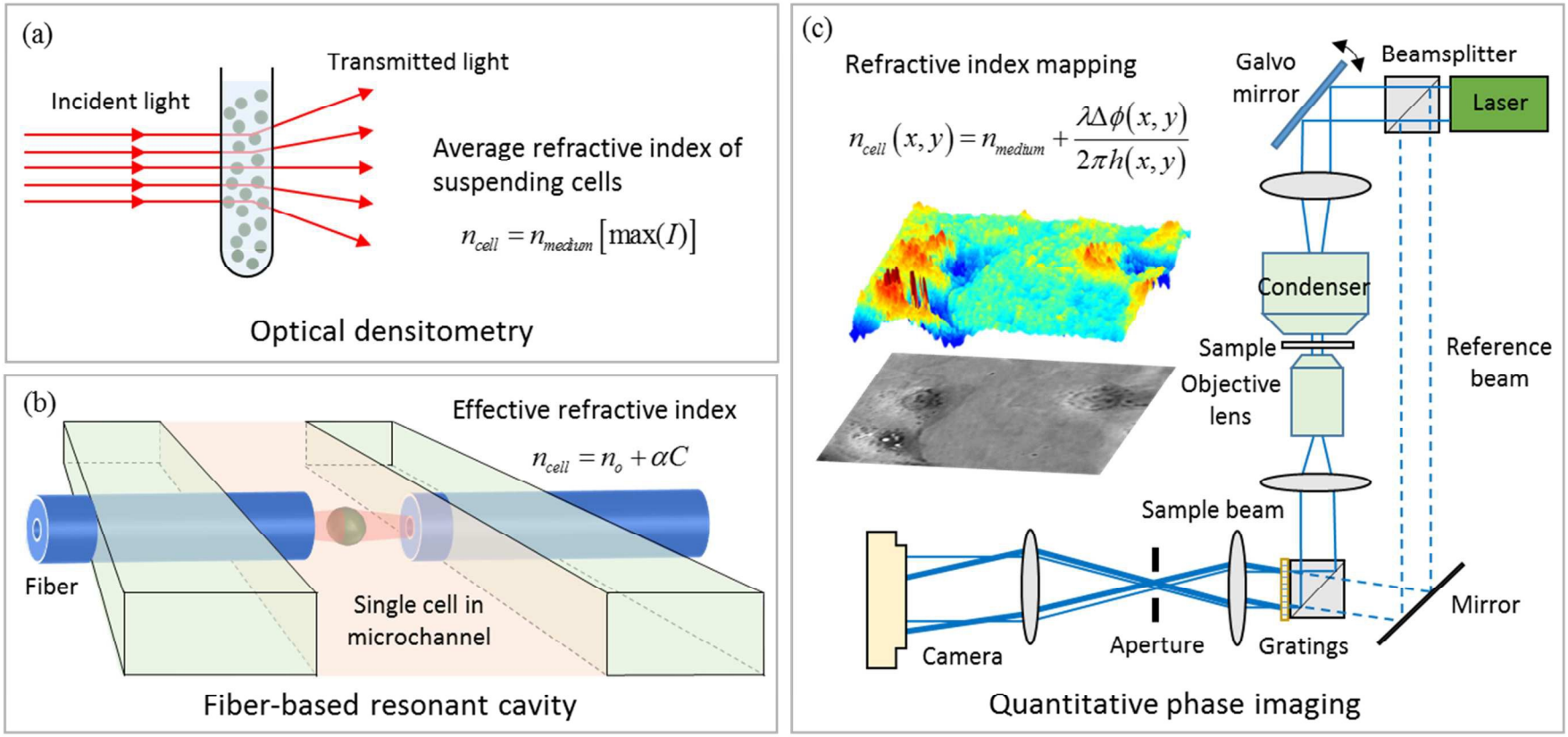

Figure 1

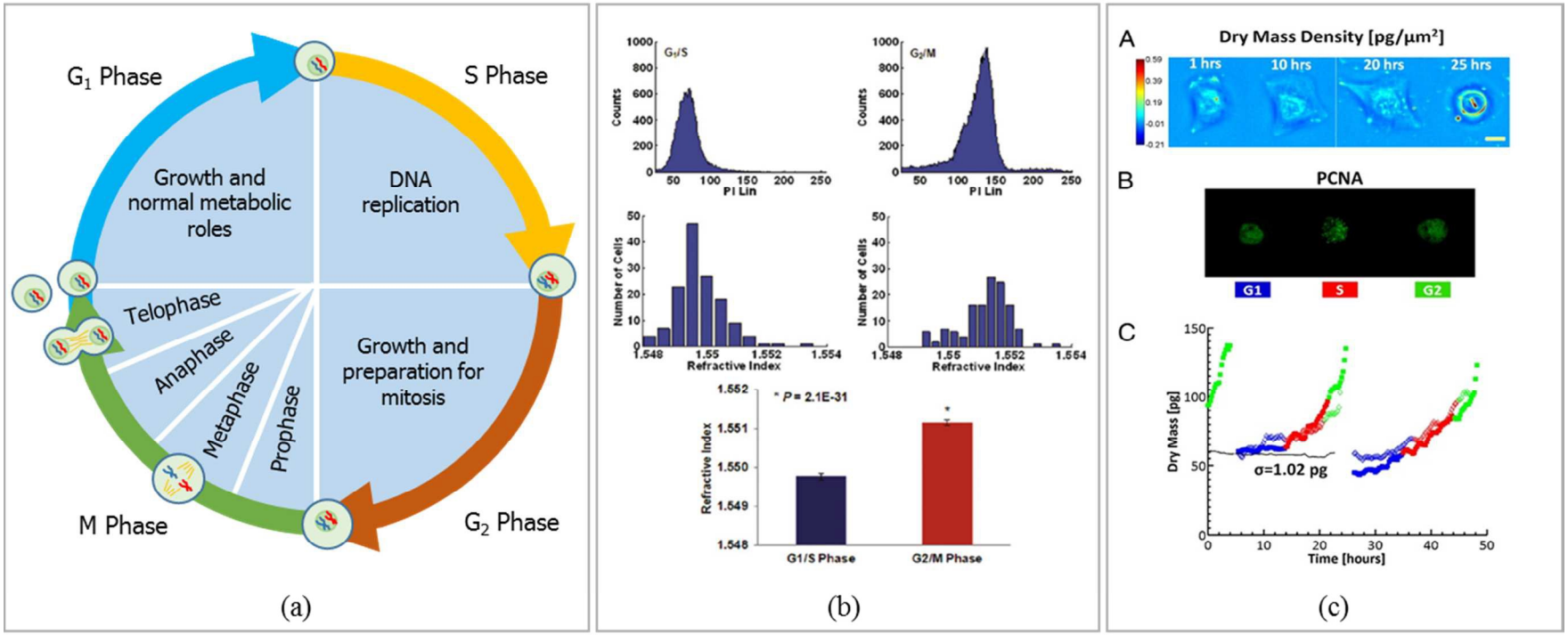

Figure 2

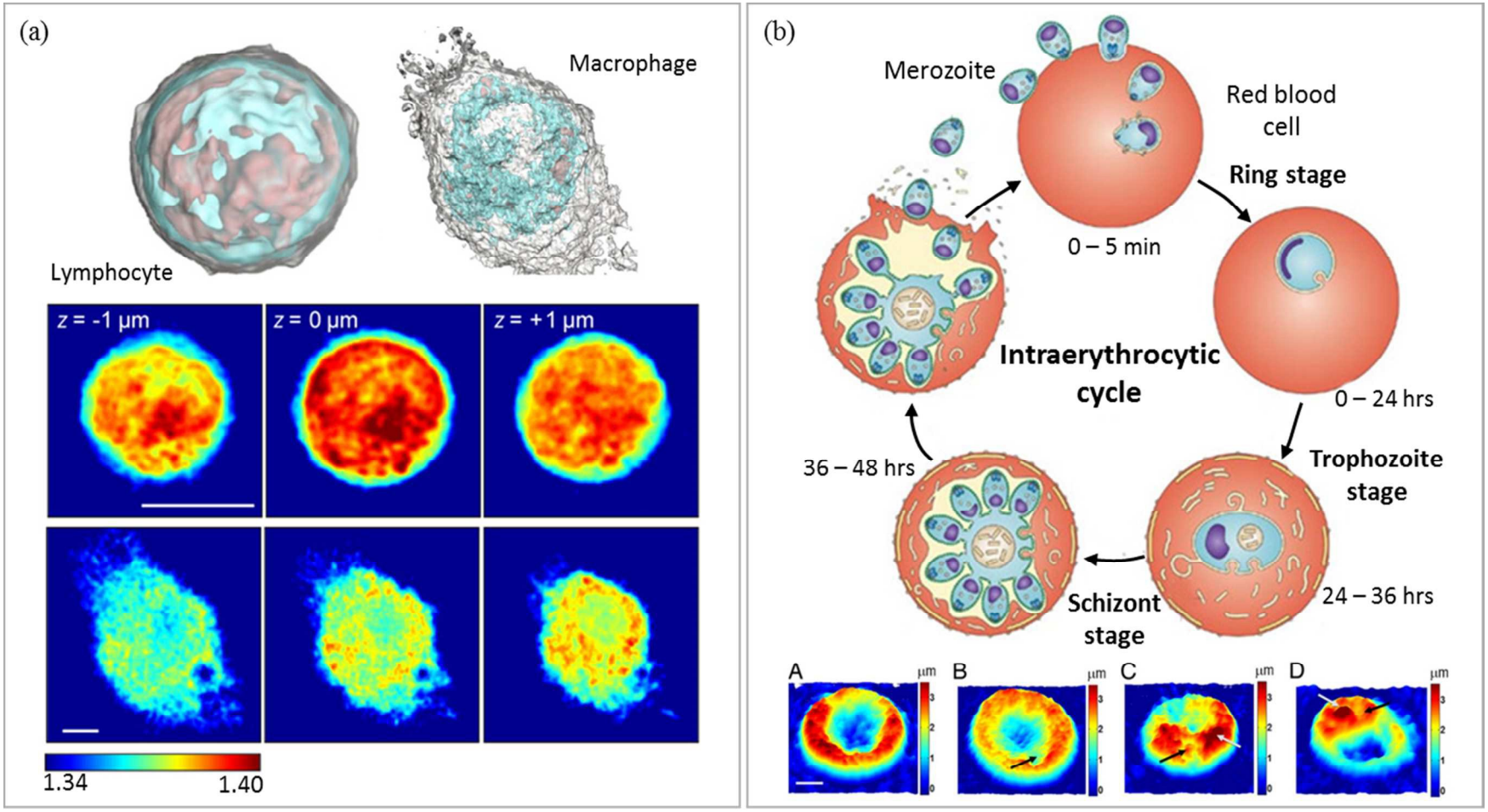

Figure 3

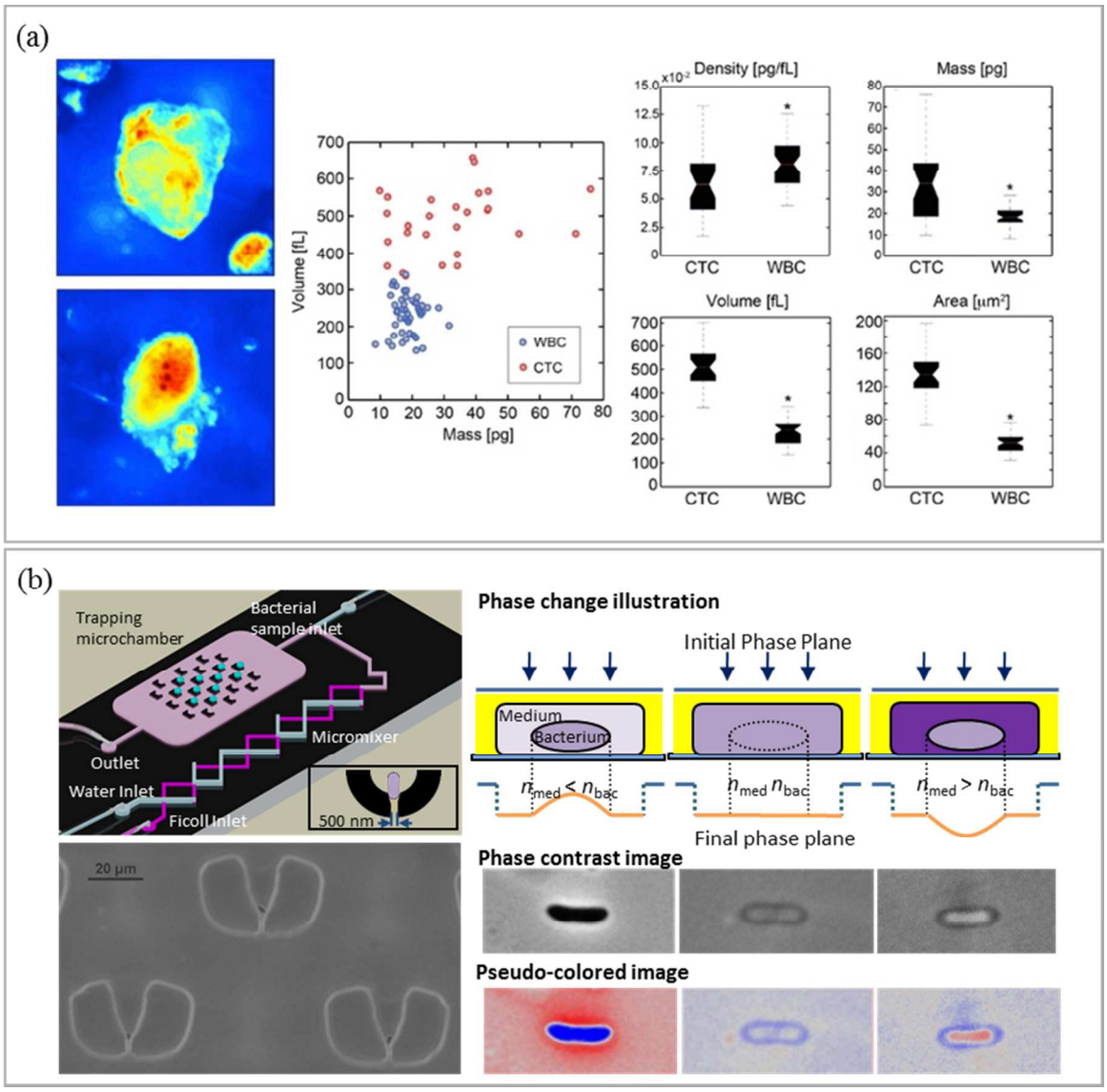

Figure 4

Table 1

Cell refractive index model	Measurement technique	Refractive index resolution (RIU)	Minimal mass density change (pg/fL)*	Spatial resolution (nm)	Refs
Average refractive index of suspending cells	Interference refractometer	3×10^{-3}	0.0163	-	[5]
	Optical densitometer	3×10^{-3}	0.0163	-	[5]
	Light scattering	10^{-2}	0.0542	-	[6]
	Light transmission and reflection	10^{-2}	0.0542	-	[7]
Effective refractive index of a single cell	Immersion refractometer	1×10^{-3}	0.0054	-	[11, 12]
	Light scattering	1×10^{-2}	0.0542	-	13]
	Laser resonant cavity	4×10^{-3}	0.0217	-	14]
	FP resonant cavity	3×10^{-3}	0.0163	-	15]
	Grating resonant cavity	1×10^{-3}	0.0054	-	16]
	Mach-Zehnder interferometer	1×10^{-3}	0.0054	-	17]
Refractive index mapping	Surface plasmon nano-optical probe	4×10^{-5}	0.0002	80	[18, 19]
	Confocal quantitative phase microscopy	4×10^{-3}	0.0217	-	[20]
	Digital holographic microscopy	1×10^{-2}	0.0542	-	[21]
		3×10^{-4}	0.0016	-	[22]
	Hilbert phase microscopy	2×10^{-3}	0.0108	1000	[23]
	Phase-shifting interferometry	9×10^{-3}	0.0488	250	[24]
		3×10^{-4}	0.0016	-	[25]
	Common-path tomographic diffractive microscopy	1×10^{-3}	0.0054	-	[26]
	Microfluidic off-axis holography	5×10^{-3}	0.0271	350	[29]
	Tomographic bright-field imaging	8×10^{-3}	0.0434	260	[30]

* $\alpha = 0.1845$ ml/g is used to calculate the minimal mass density change to be detected by the respective measurement techniques.

Table 2

Organelles/intracellular matters	Refractive index	References
Cytosol	1.360 – 1.390	[28]
Nucleus	1.355 – 1.365	[28]
Nucleolus	1.375 – 1.385	[28]
Mitochondria	1.400 – 1.420	[31]
Lysosome	1.600	[32]